Electronic Supplementary Material (ESI) for Nanoscale.
This journal is © The Royal Society of Chemistry 2014

Electronic Supplementary Information

Thermoelectricity at the Molecular Scale: Large Seebeck Effect in Endohedral Metallofullerenes

See Kei Lee,[a] Marius Bürkle,[b] Ryo Yamada,[a] Yoshihiro Asai[b] and Hirokazu Tada[a]

[a]Graduate School of Engineering Science, Osaka University, 1-3 Machikaneyama, Toyonaka, Osaka, 560-8531, Japan
[b]Nanosystem Research Institute, National Institute of Advanced Industrial Science and Technology (AIST), Umezono 1-1-1, Tsukuba Central 2, Tsukuba, Ibaraki 305-8568, Japan

Conductance histogram

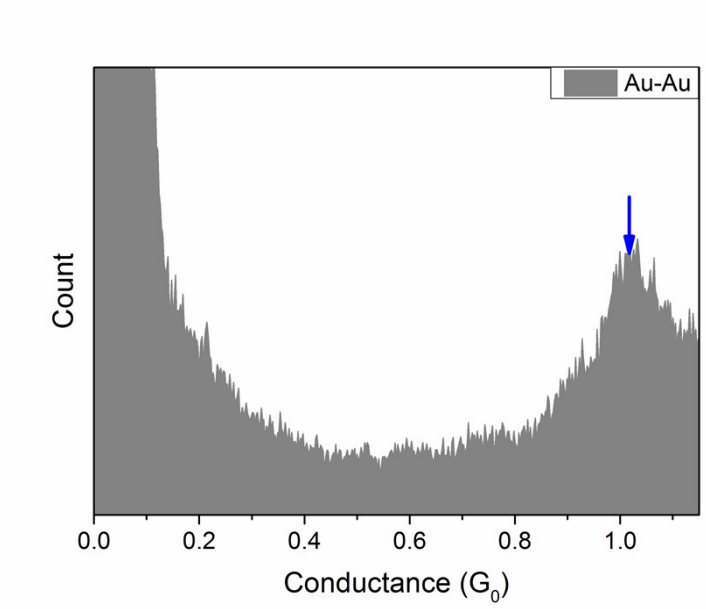

Fig. S1 Conductance histogram of bare substrate.

Fig. S1 shows the conductance histogram obtained for bare Au substrate (without presence of molecule).

Electronic Supplementary Material (ESI) for Nanoscale.

Example of set of time domain data

Here we present a representative set of current and voltage data for an Au-Ce@C_{82}-Au molecular junction measured at ΔT = 10 K. The current and voltage measurements were alternatively measured as described in the text. Majority of the measured voltage values were negative. We, however, occasionally observed both positive and negative thermoelectric voltage (TEV) values for the endohedral metallofullerene (EMF) molecules (Gd@C_{82} and Ce@C_{82}) during our measurement as indicated by the arrows in Figure S2. Although we have not been able to identify the structures giving rise to the positive TEV in the theoretical models, one of the meta-stable configurations of the junctions might be attributed to the positive TEV.

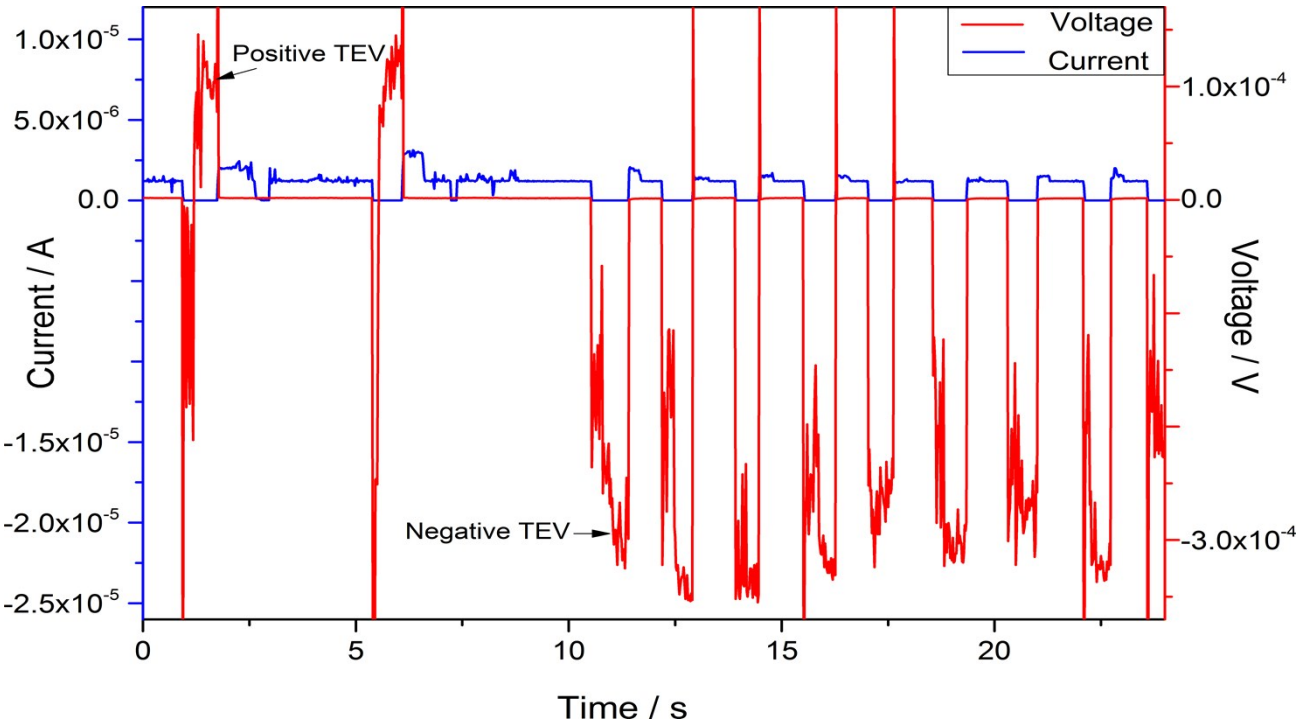

Fig. S2 Voltage and current as a function of time graph for Au-Ce@C82-Au junctions when the tip was held at ΔT = 10 K.

Electronic Supplementary Material (ESI) for Nanoscale.

Density functional theory calculations

The geometrical and electronic structure of the molecular junctions was obtained in the framework of density functional theory (DFT). We employed the TPSSh functional[1,2] with empirical dispersion corrections to the total ground-state energy accounting for long-range Van der Waals interaction to describe the metal-molecule interaction correctly.[3] As bases, def2-SV(P)[4] and the respective Coulomb fitting bases[5] was used.

Modeling of the contact geometries

For all three EMFs, we assume that the structures of the C_{82} cage is given by the stable isomer of the gas phase molecule, namely C_2 for the bare C_{82} molecule and C_{2v} for Gd@C_{82} and Ce@C_{82} respectively. The molecular junctions are modeled by finite "extended central cluster" (ECC) consisting of the EMF and large parts of the metal electrodes to ensure the proper alignment of molecular levels with respect to the electrodes Fermi energy, E_F.
While it would be preferable to investigate a large range of possible binding geometries this is unfortunately computationally not feasible, we therefore restrict ourselves to two representative geometry reasonable for the experimental setup. In our experiments the EMFs are firstly adsorbed on the Au-surface and then contacted directly by the STM tip to from a stable junction. Along this lines we assume an approximately adiabatic formation of the junction. The choice of the initial binding motif follows the idea that the binding of fullerenes to the Au surface is mainly given by adsorption through van der Waals interactions[6,7] which makes it reasonable to assume that it will tend to orient approximately with either a five- or six membered carbon ring parallel to the Au-surface and not bind to e.g. a single or under coordinated adatom.[6-8] Along this lines we start from two binding motifs with either a five-membered (geometry G-I) or a six-membered (geometry G-II) carbon ring facing the Au surface. The structures are then fully optimized. The procedure adopted to determine the structure of the ECC, as summarized in Figure S3, follows the idea of an adiabatic junction formation and is identical for all three EMFs. First the EMF is connected to three apex atoms of a single Au <111> cluster with 86 Au atoms at ideal FCC lattice positions. The EMF and the apex atoms are fully relaxed until the total energy and the maximum norm of the Cartesian gradient are converged to a precision of better than 10^{-6} a.u. and 10^{-4} a.u., respectively. To construct the ECC, a second Au <111> cluster with identical crystal orientation is attached; its position is given by inversion of the first cluster on the geometrical center of mass of the EMF. Then once again, the EMF and the 6 apex atoms are relaxed.

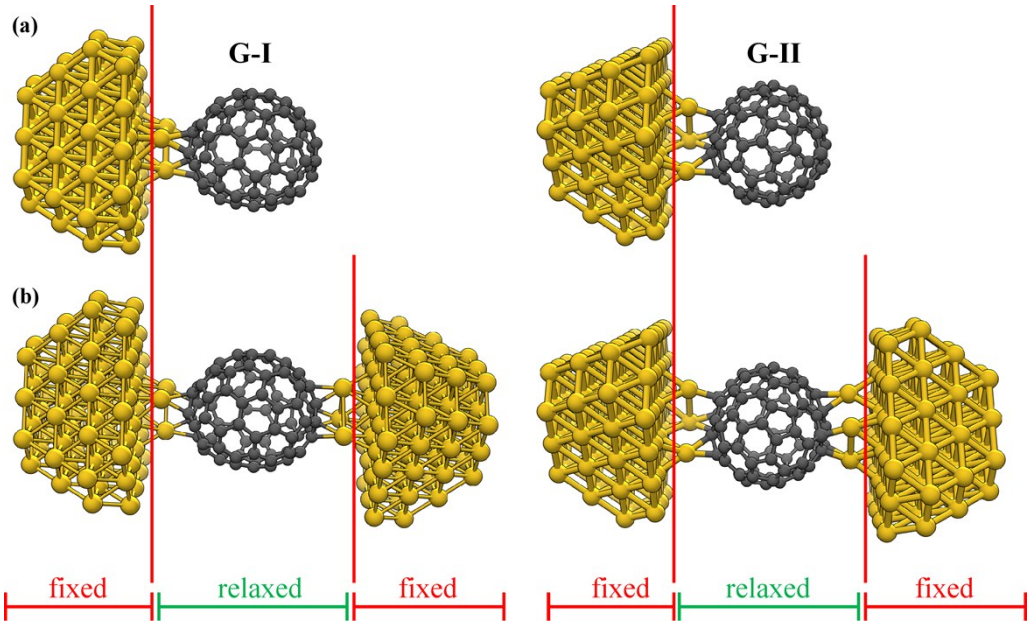

Fig. S3 Procedure used to set up the contact geometry, here exemplarily displayed for Au-C_{82}-Au.

Relation between gas phase electronic structure and transmission

To clarify the influence of the lanthanide atoms on the transport, we connect the gas phase electronic structure of the fullerenes to the obtained transport properties. Incorporating the lanthanides into the C_{82} cage result in a transfer of partial negative charge from the lanthanide atom onto the C_{82} cage and the symmetry of the stable isomer changes from C_2 for C_{82} to C_{2v} for Gd@C_{82} and Ce@C_{82}.[9-11] This will cause a change in the character of the frontier orbitals involved in the transport. Additionally

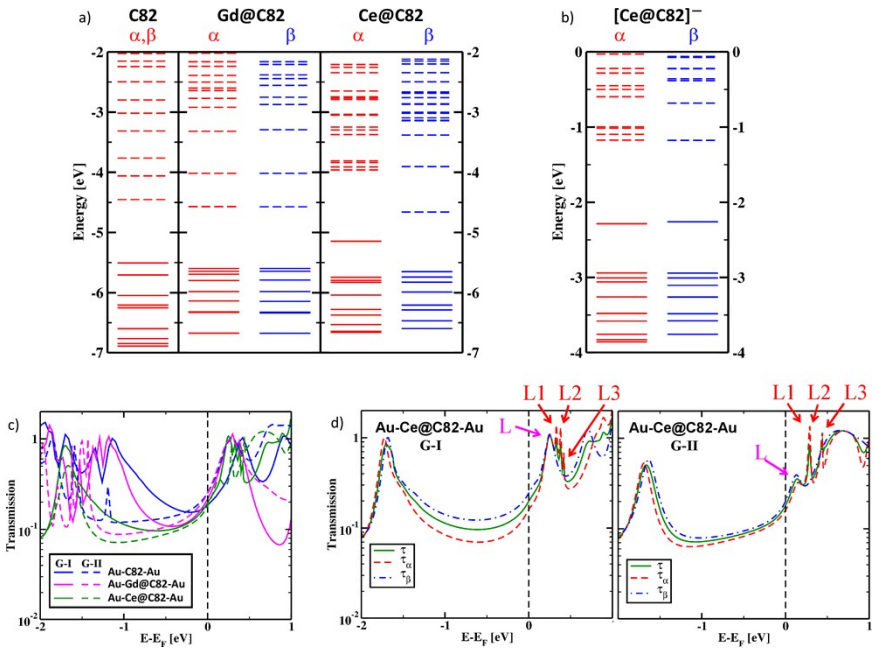

Fig. S4 a) Single electron energy levels of C_{82}, Gd@C_{82}, and Ce@C_{82} molecules in gas phase. b) Single electron energy levels of the closed-shell anion $[Ce@C_{82}]^-$. c) Transmission spectra of C_{82}, Gd@C_{82} and Ce@C_{82}. Here the transmission is given as the average of the transmission in the two spin channels α and β. d) Spin resolved transmission spectra for Au-Ce@C_{82}-Au. L denotes the position of the resonance due to the energy degenerate α- and β-LUMO, while L1-3 denotes the resonances due to the α- LUMO-1, LUMO-2 and LUMO-3, respectively.

the outer f-shells of Gd and Ce give rise to a non-trivial spin polarized ground state with a spin multiplicity of M = 7 for Gd@C_{82} and M = 2 for Ce@C_{82} respectively.[9-12] It has to be noted that although electron correlation can play an important role for the heavy lanthanide atoms, we can expect that the energy level relevant for transport are all well described at a DFT (DFT+Σ) level as they are mainly localized on the C_{82} cage.

The corresponding single electron energy levels are given in Fig. S4a. As expected, C_{82} is in a closed-shell system. For Gd@C_{82}, although the molecule is in a high-spin state, the orbitals around the HOMO-LUMO gap are essentially closed-shells with identical energies for the α-shells (spin-up) and β-shells (spin-down). On the other hand, the orbital energies for Ce@C_{82} differ strongly between the α- and β-shells. Due to the open electron shell of the neutral radical Ce@C_{82} the unoccupied α-LUMO can be populated relatively easily, reducing the molecule to its closed-shell anion $[Ce@C_{82}]^-$ with the gas phase electronic structure given in Figure S4b. As the reduction of Ce@C_{82} to its anion will stabilize the molecule when connected to Au adatoms of the electrodes, we can expect that the molecule inside the junctions is approximately in its anionic form $[Ce@C_{82}]^-$. To confirm this, we calculated the charge transfer from the Au electrodes onto Ce@C_{82} by means of the Mulliken charge analysis (MCA)[13] and the natural population analysis (NPA)[14], both yielding consistently a charge transfer of around -1.0 |e| (Q_{MCA} = -0.8 |e|, Q_{NBA} = -1.1 |e| for G-I and Q_{MCA} = -0.9 |e|, Q_{NBA} = -1.3 |e| for G-II) onto the C_{82} cage and almost equal charge in both shells, whereas the charge on the encapsulated Ce atom remains basically unchanged from its gas-phase value. This indicates that the α-LUMO is indeed populated once the molecule is brought into contact, leaving the molecule approximately in its anionic form $[Ce@C_{82}]^-$. Moreover, although we do not account for solvent effects in our calculations, it has to be pointed out that the dimethylformamide-based solvent used in our experiments will independently reduce and stabilize Ce@C_{82} to its anion.[15] The single electron levels can be correlated with the resonances in the transmission spectra shown in Figure S3c. For Ce@C_{82}, the spin resolved transmission spectra given in Figure S3d can be well understood in terms of the single electron levels of $[Ce@C_{82}]^-$ (Fig. S3b), while it is not consistent with the electronic structure of the neutral radical Ce@C_{82} (Fig. S3a). As suggested from the single electron levels of $[Ce@C_{82}]^-$ (Fig. S3b), the HOMO resonance for both spin channels are located at almost identical energies. Similar energy degeneration holds for the α- and β-LUMO. In the α-channel, however, there are 3 additional resonances slightly above the LUMO due to α-LUMO-1, LUMO-2 and LUMO-3, which are absent for β-spin. For G-II we cannot individually resolve all the resonances as they are presumably so close in energy, giving rise to a single peak with a transmission larger than 1.

DFT+Σ

It is well known that DFT-based transport calculations tend to overestimate the conductance[16], which is largely related to the deficiency to accurately describe the energy gap and level alignment of molecules at surfaces[17] due to self-interaction errors and missing long-range correlation within approximate DFT schemes. The DFT+Σ approach introduced recently has been shown to

improve the agreement with the experiments for both conductance and thermopower.[16-18] The details of our DFT+Σ implementation can be found in reference 18.

Here we will just shortly introduce the basic idea of the DFT+Σ approach, that is to correct both, the underestimation of the HOMO-LUMO gap of the gas-phase molecule as well as the missing long-range correlation in an approximate, yet parameter free, manner. Essentially the energy levels of the molecular subspace H^{M} of the total Hamiltonian H^{ECC} of the contacted molecule are shifted such that we account for both errors. Firstly, the underestimation of the HOMO-LUMO gap of the gas-phase molecule is corrected by shifting the energies of the occupied levels such that the energy of the HOMO (ε_H) corresponds to the negative ionization potential (IP) and respectively the unoccupied (virtual) levels are shifted such that the LUMO (ε_L) energy corresponds to the negative electron affinity (EA). The IP=*E(Q=+e)-E(Q=0)* and EA=*E(Q=0)-E(Q=-e)* are computed with ΔSCF by the difference of the total energies of the neutral molecule *Q=0* and its charged *Q=±e* species.

To account for the missing long-range correlation we adopt a classical image charge module as described in references 18 and 19. Basically the molecule is approximated by point charges (Mulliken brutto charges of the HOMO and LUMO) at the atomic positions placed between two perfectly conducting infinite surfaces, for such a setup the corresponding changes in the potential energy can be calculated analytically.[18] The shift of the occupied levels is denoted by Δ_{occ} and the shift of the unoccupied levels by Δ_{virt}. The total shift of the occupied levels is given by $\Sigma_{occ}=-IP-\varepsilon_H+\Delta_{occ}$ and the unoccupied ones are shifted by $\Sigma_{virt}=-EA-\varepsilon_L+\Delta_{virt}$.

In Table S1 we have summarized the level shifts for the molecules considered in this study. For Au-Ce@C82-Au we did explicitly consider the shifts for each spin channel α and β separately, however they are essentially identical for both spins.

	$-IP-\varepsilon_H$	Δ_{occ}	Σ_{occ}	$-EA-\varepsilon_L$	Δ_{virt}	Σ_{virt}
Au-C82-Au (G-I)	-1.21	0.72	-0.49	1.21	-0.82	0.39
Au-C82-Au (G-II)	-1.21	0.74	-0.47	1.20	-0.83	0.37
Au-Gd@C82-Au (G-I)	-1.20	0.74	-0.46	1.20	-0.78	0.42
Au-Gd@C82-Au (G-II)	-1.19	0.76	-0.43	1.22	-0.78	0.44
Au-Ce@C82-Au (α) (G-I)	-1.22	0.75	-0.47	1.22	-0.84	0.38
Au-Ce@C82-Au (β) (G-I)	-1.20	0.74	-0.46	1.22	-0.84	0.38
Au-Ce@C82-Au (α) (G-II)	-1.22	0.75	-0.47	1.20	-0.84	0.36
Au-Ce@C82-Au (β) (G-II)	-1.19	0.73	-0.46	1.19	-0.84	0.35

References

1. J. Tao, J.P. Perdew, V.N. Staroverov and G.E. Scuseria, *Phys. Rev. Lett.*, 2003, **91**, 146401.
2. V.N. Staroverov, G.E. Scuseria, J. Tao and J.P. Perdew, *J. Chem. Phys.*, 2003, **119**, 12129.
3. S. Grimme, *J. Comput. Chem.,* 2006, **27***,* 1787-1799.
4. F. Weigend and R. Ahlrichs, *Phys. Chem. Chem. Phys.,* 2005**, 7**, 3297-3305.
5. F. Weigend, *Phys. Chem. Chem. Phys.,* 2006, **8**, 1057-1065.
6. E. I. Altman and R. J. Colton, *Surf. Sci.*, 1992, **279**, 49.
7. I. Hamada and M. Tsukada, *Phys. Rev. B*, 2011, **83**, 245437.
8. L.-L. Wang and H.-P. Cheng, *Phys. Rev. B*, 2004, **69**, 165417.
9. A. Sebetci and M. Richter, *J. Phys. Chem. C,* 2010, **114**, 15.
10. L. Senapati, J. Schrier and K. B. Whaley, *Nano Lett.,* 2004, **4**, 2073.
11. K. Muthukumar and J. A. Larsson, *J. Phys. Chem. A,* 2008, **112,** 1071.
12. J. Ishikawa, T. Miyahara, Y. Hirato, H. Ishii, T. Kodama, K. Kikuchi, T. Nakamura, K. Kodama, D. Asakura and T. Koide, *J. Electron. Spectrosc. Relat. Phenom.,* 2011, **184**, 284.
13. R. S. Mulliken, *J. Chem. Phys.* 1955, **23**, 1833.
14. A. E. Reed, R. B. Weinstock and F. Weinhold, *J. Chem. Phys.,* 1985, **83**, 735.
15. S. P. Solodovnikov and S. F. Lebedkin, *Russ. Chem. Bull*., 2003, **52**, 1111.
16. S.Y. Quek, L. Venkataraman, H.J. Choi, S.G. Louie, M.S. Hybertsen and J.B. Neaton, *Nano Lett.*, 2007, **7**, 3477.
17. J.M. Garcia-Lastra, C. Rostgaard, A. Rubio and K.S. Thygesen, *Phys. Rev. B*, 2009, **80**, 245427.
18. L. A. Zotti, M. Bürkle, F. Pauly, W. Lee, K. Kim, W. Jeong, Y. Asai, P. Reddy and J. C. Cuevas, *New J. Phys.* 2014, **16** (1) 015004.
19. D.J. Mowbray, G. Jones and K.S. Thygesen, *J. Chem. Phys.*, 2008, **128**, 111103.